

EVALUATION OF LIQUID HYDROGEN CONDITIONING CONCEPTS FOR AIRCRAFT ENGINES EMPLOYING EXHAUST-GAS WASTE-HEAT RECOVERY

Philip Kirschnek[1], Alexander Görtz[2], Marc Schmelcher[2], Fynn Thilker[1] & Jannik Häßy[2]

[1]FH JOANNEUM GesmbH - University of Applied Sciences, Institute of Aviation, 8020 Graz, Austria
[2]German Aerospace Center (DLR), Institute of Propulsion Technology, 51147 Cologne, Germany

Abstract

Hydrogen-powered aviation has re-emerged as a promising long-term option for reducing the climate impact of air transport. The shift in propulsion technologies is caused by the increasing demand in clean aviation. When stored in liquid form, hydrogen requires dedicated conditioning systems to manage cryogenic temperatures, pressurization, and heat transfer prior to combustion. This paper investigates the thermodynamic behavior of multiple liquid hydrogen conditioning architectures for fuel-burning jet engines, with emphasis on exhaust-gas waste-heat recovery. Several hydrogen conditioning architectures are modeled using the virtual engine framework GTlab, employing exhaust-gas waste-heat recuperation of the engine's core as the primary heat source, complemented by thermal energy from the engine oil and compressor bleed air utilized at the environmental control system. A closed nitrogen secondary fluid cycle is implemented to enable safe and flexible heat transfer between engine heat sources and hydrogen. Design and off-design parameter and sensitivity studies are evaluated to assess the impact on component sizing, hydrogen injection temperatures, pressurization devices, and overall conditioning performance. The results highlight key trade-offs between achievable hydrogen injection temperatures in the range of $300\,\mathrm{K}$ to $400\,\mathrm{K}$ at the consumer, heat exchanger compactness, and mechanical power input for fluid delivery, providing guidance for early-stage design of hydrogen-fuel systems for aero-engines implementing exhaust-gas waste-heat recovery.

Keywords: hydrogen conditioning, jet engines, heat exchanger, thermal management, exhaust-gas recuperation

1. Introduction

The environmental impact of aviation and its contribution to global greenhouse gas emissions [1, 2] continue to drive research into alternative propulsion technologies and fuels, giving rise to synthetic aviation fuels alongside hydrogen as an energy carrier. Early work by Lockheed and NASA investigated hydrogen-fueled gas turbine engine concepts, covering the design problems of liquid hydrogen (LH_2) propulsion [3]. Subsequent research programs, including CRYOPLANE, explored aircraft-level modifications required for LH_2 operation [4], while more recent initiatives such as Airbus' ZEROe project focus primarily on hydrogen fuel cell propulsion for short- and medium-range aircraft [5]. Across these and various additional studies, hydrogen thermal management is consistently identified as a critical enabling technology (cf. [3, 4, 5, 6, 7, 8, 9]).

For fuel-burning hydrogen engines, LH_2 must be pressurized, vaporized, and heated to sufficiently high injection temperatures to ensure stable combustion, avoid heat exchanger (HX) icing, and maintain safe operation of engine subsystems. Several concepts to condition hydrogen have been proposed in literature, employing different combinations of heat exchangers and engine heat sources [9,

10, 11, 12]. These studies demonstrate the feasibility of individual approaches for waste-heat recovery (WHR) of systems with significant thermal loads applicable for heating hydrogen. The thermodynamic potential of this approach is substantial: heating hydrogen from cryogenic tank conditions to near-exhaust temperatures raises its specific enthalpy by approximately $10\,\%$ of its lower heating value, with a corresponding reduction in specific fuel consumption in a pressure-loss-free system [13, 14].

A systematic evaluation of LH_2 conditioning architectures that explicitly combine multiple engine heat sources within a secondary fluid based thermal management framework remains limited in existing work. This work addresses the current research gap by investigating defined LH_2 conditioning architectures for hydrogen-burning aircraft engines applicable for single-aisle airliners. The primary focus is on WHR from the exhaust-gas (EG) stream of the engine's core, complemented by thermal energy extracted from the engine-oil and compressor bleed-air. A closed secondary fluid cycle is employed to transfer heat between engine heat sources and hydrogen, avoiding direct exposure of hydrogen at the exhaust-gas HX, increasing safety margins. The conditioning systems are implemented within the virtual-engine framework GTlab [15], developed by the German Aerospace Center (DLR), which supports propulsion-system design and simulation across multiple levels of fidelity. A variation of hydrogen injection temperatures during cruise flight is examined to assess the influence on system design level of the hydrogen conditioning framework. The consequent impact on off-design conditions is evaluated. The analysis targets the influence of varying thermal loads and hydrogen mass flow rates (MFRs) on heat exchanger performance and sizing trends, alongside the operating behavior pressurization components. By comparing different conditioning environments and architectures, this work contributes to early-stage design considerations and the evaluation of LH_2 conditioning and thermal management systems for future aircraft applications. The work of Görtz et al. [16] builds on the findings of this study and integrates the described liquid hydrogen conditioning methods directly into the performance model of a turbofan engine, where the effect of conditioning performance and efficiency in terms of specific fuel consumption is addressed [16].

2. Hydrogen Conditioning Architectures

In this work, hydrogen is supplied from a cryogenic tank at $20\,\mathrm{K}$ with an array of low- and high-pressure pumps operating at $5\,\mathrm{bar}$ and $60\,\mathrm{bar}$, respectively. For application at the consumer, i.e. a combusting aero-engine, hydrogen temperatures in the range of $150\,\mathrm{K}$ to $250\,\mathrm{K}$ are required at the combustor, ensuring proper mixing with the airstream [17]. Modern aircraft engines provide large amounts of thermal energy in various subsystems, which can be utilized for hydrogen conditioning. While combustion temperatures exceed $2500\,\mathrm{K}$ [18], safety and packaging constraints prevent direct use of the combustion chamber as a heat source. Other sources contributing thermal loads include the previously mentioned EG stream, engine oil, and bleed-air cooling in the primary HX of the environmental control system (ECS) [12]. Pre- or intercoolers in the compressor stages can also serve as potential heat sources by recovering energy from the cooling of pressurized air [19, 20], decreasing specific fuel consumption in take-off by up to $4\,\%$ [21], but they require significant changes to the compressor design. Thus, the main focus during this work is on extracting thermal energy from the

- engine oil,
- bleed-air,
- and exhaust-gas,

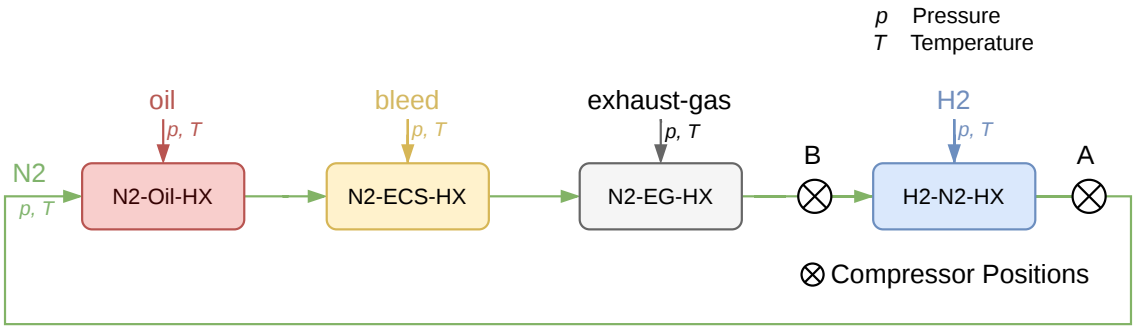
as the first two require cooling independent of the propulsion system. Among the candidate heat sources, the exhaust stream offers the highest source temperature and therefore the smallest required heat transfer area for a given heating duty [13], making it the primary energy source for hydrogen conditioning in this work.

To transfer heat into the hydrogen via a secondary fluid network, the heat transfer fluid needs to

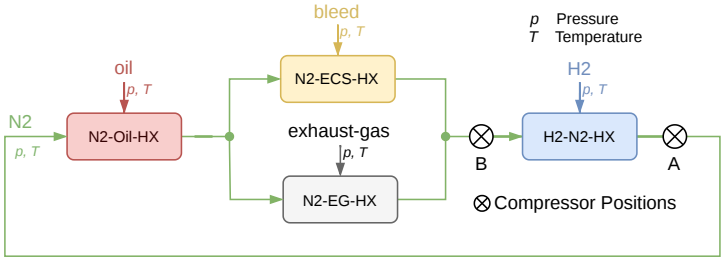
fulfill several requirements: it must neither be toxic nor flammable and explosive during leak scenarios; the minimum operating temperature should remain above the boiling curve, ensuring single phase operation; thermophysical properties must be suitable for forced convection flows with high heat transfer requirements. Among viable fluids, including helium, argon, and nitrogen (N_2), the latter was employed due to its accessibility and greater operating range, as a preliminary analysis has shown. The defined heat exchangers will be referred to as N2-Oil-HX, N2-ECS-HX, and N2-EG-HX in the order listed previously. Heat is transferred to the hydrogen at the H2-N2-HX.

The arrangement of the heat exchangers within the fluid network defines the effectiveness of heat transfer and the resulting thermodynamic conditions of the respective fluids, as the operating temperature of the heat exchangers affects their performance. Heat exchanger sizing is affected, in addition to auxiliary power demand. Three distinct network topologies, with a simplified visualization shown in Figure 1, are investigated in this work:

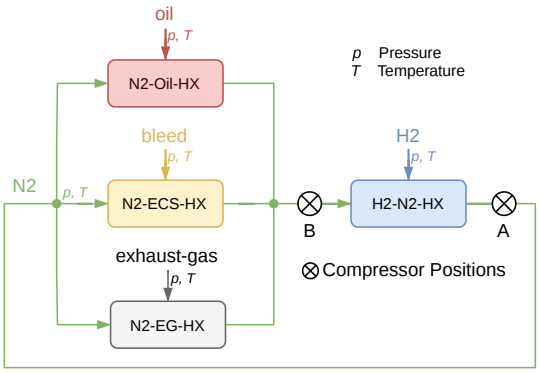
- **Serial** arrangement (*S*): all three heat sources are connected in series, reducing flow control flexibility (Figure 1a)
- **Semi-Parallel** arrangement (*SP*): the oil-cooler is placed in series upstream of the ECS- and EG-HXs, which operate in parallel, improving condensation and icing resistance of humid air within the ECS and EG, as the nitrogen is preconditioned (Figure 1b)
- **Parallel** arrangement (*P*): the oil-cooler, ECS- and EG-HXs operate in parallel, allowing independent mass flow control via valves (Figure 1c)



(a) Serial HX arrangement.



(b) Semi-Parallel HX arrangement.



(c) Parallel HX arrangement.

Figure 1 – Simplified sketch of studied hydrogen conditioning architectures with the H2-, oil-, ECS-, and EG-HX and compressor positions.

Pressurization of the nitrogen cycle and continuous fluid delivery is ensured by a compressor. Compressor positioning within the fluid system will affect power consumption, thermal energy input into the fluid, as well as the operating behavior and flexibility in off-design conditions. Two distinct positions are examined – one at the lowest operating temperatures (after the H2-N2-HX – compressor

position *A*); one at the highest operating temperature (after the HX array heating the N_2 – compressor position *B*), additionally outlined in Figure 1.

With the serial arrangement, the nitrogen first passes through the oil-cooler. At the oil-cooler, the oil temperature is reduced to fulfill subsequent cooling demands within the engine, whereas the nitrogen temperature is increasing. Afterward, the nitrogen passes through the N2-ECS-HX, where the required bleed air cooling rate for later use in the environmental control system is specified; thus, it further increases the temperature of the nitrogen. A heat exchanger placed in the engine's core stream lastly increases the nitrogen temperature, which emits heat at the H2-N2-HX to raise the hydrogen's temperature to specified inlet conditions. The serial architecture is least flexible in terms of mass flow and energy control.

The semi-parallel splits the nitrogen flow after the oil-cooler to have minimum inlet temperature conditions at both the N2-ECS-HX and N2-EG-HX, allowing flexible mass flow ratios improving performance in off-design conditions, where a shift in thermal energy dissipation might be required.

The parallel setup enables full mass flow control as a function of the operational condition, directly controlling the amount of gaseous nitrogen passing through the oil-cooler, N2-ECS-, and N2-EG-HX. Higher flexibility in terms of flow control, however, will increase the complexity of flow regulation, with multiple valves and feed lines required, while considering redundancy requirements of the thermal management system.

2.1 Boundary Conditions and Fluid Models

The simplified hydrogen conditioning architectures shown in Figure 1 are modeled in GTlab. The hydrogen system is established starting from a high-pressure pump, with the inlet properties specified. The boundary conditions for the bleed-air and exhaust-gas are derived from an in-house engine performance simulation representative of a short-to-medium-range single-aisle airliner (cf. [22]). The engine-oil system is developed as a closed loop, passing through gear pumps and components accounting for pressure losses within the engine.

Table 1 summarizes the mass flow rate $\dot{m}$, temperature T, and pressure p of each fluid at its respective starting point within the modeled conditioning architectures. Herein, the cruise (CR) condition is treated as the design point, to which each system and component is sized. The maximum take-off (MTO) case defines the analyzed off-design case due to peak thermal loads, simulating the performance based on the architecture's design, evaluated in CR. The working fluids obtain real gas properties derived from the CoolProp [23] fluid library. As the fluids are either fully liquid or gaseous and thus outside of the wet steam region, defining the pressure and temperature is sufficient.

Table 1 – Boundary conditions at the fluids' starting points. $f(n)$, $f(a)$ and $f(m)$ denote dependence on the compressor speed, architecture and mass flow rate, respectively, and are solved by the defined equation system described in Section 2.2.

	H_2		N_2		Oil		ECS		EG	
OP	CR	MTO	CR	MTO	CR	MTO	CR	MTO	CR	MTO
$\dot{m}$ (kg/s)	0.118	0.32	2.7	f(n)	2.0	f(n)	0.4	0	1.6	3.8
T (K)	25	25	f(a)	f(m)	413	413	835	0	640	796
p (bar)	5	5	50	80	4	4	7	0	0.32	0.32

Hydrogen enters the HP pump at $25\,\mathrm{K}$ and $5\,\mathrm{bar}$, with mass flow rates of $0.118\,\mathrm{kg/s}$ in CR and $0.32\,\mathrm{kg/s}$ in MTO, slightly below the values reported by Brewer [3] for a comparable subsonic hydrogen-powered aircraft. The target hydrogen injection pressure is set to $60\,\mathrm{bar}$ to remain above high-pressure compressor exit pressures. Nitrogen is pressurized to $50\,\mathrm{bar}$ in CR to stay within the H2-N2-HX's structural limits, at a nominal design MFR of $2.7\,\mathrm{kg/s}$. The oil lubrication system is modeled with constant fluid properties based on the Exxon dataset [24], (covering a temperature range of $233\,\mathrm{K}$

to $474\,\mathrm{K}$,) at $413\,\mathrm{K}$ and $4\,\mathrm{bar}$. ECS bleed-air is extracted from the engine's compressor at $835\,\mathrm{K}$ and $7\,\mathrm{bar}$ with a MFR of $0.4\,\mathrm{kg/s}$. $10\,\%$ of the core exhaust gas is diverted to the N2-EG-HX, at $640\,\mathrm{K}$ and $0.32\,\mathrm{bar}$ for CR conditions.

Heat flow rate targets are derived from calculated engine performance demands. In CR, the oil-cooler and N2-ECS-HX dissipate $157\,\mathrm{kW}$ and $76\,\mathrm{kW}$, respectively. Oil heat dissipation increases to $380\,\mathrm{kW}$ as a result of high engine loads in MTO, while the ECS is assumed to be inactive. To enable a consistent comparison between architectures, the N2-EG-HX heat flow rate is fixed at $1\,\mathrm{MW}$ in MTO, defining the attainable H_2 injection temperature in off-design.

System constraints are dominated by N2-ECS-, and especially N2-EG-HX icing, since water vapor is a major combustion byproduct and condenses onto cold HX surfaces, demanding nitrogen temperatures at the HXs' inlets above $273\,\mathrm{K}$. Further limits arise from the operational range of the pressurization devices with risks of surge and choke, as well as the hydrogen auto-ignition temperature of approximately $773\,\mathrm{K}$ [25]. Pressure losses resulting from ducting and flow control are held constant in design and scaled with the square of the MFR in off-design.

2.2 Equation System and Mathematical Background

An equation system is defined in GTlab, forming the mathematical foundation for the design and off-design solvers of the conditioning architectures. The solver iterates an independent variable until a predefined dependent parameter reaches its target value. Once all targets are satisfied simultaneously, the calculator is converged. An exemplary pair is the H2-N2-HX heat flow rate as independent variable and the hydrogen injection temperature as the dependent target. Independent variables include component pressure ratios, heat flow rates, mass flow rates, and relative rotational speeds, whereas targets include the hydrogen injection conditions, the nitrogen temperature upstream of the N2-EG-HX to limit icing, and compensation of pressure losses by the compressor of the nitrogen cycle.

In design, heat exchangers and pressurization devices are dimensioned to meet their target requirements at the main operating point, according to the pressure ratio for the compressor or the heat flow rate of the EG recuperator as an example. In off-design, the evaluated geometrical properties are fixed, and the operating points of the pumps and compressors are shifted according to their map. The compressor operating point, for example, is shifted by adjusting the shaft speed and the relative map position β along a constant speed curve. Selecting appropriate independent-dependent pairs is non-trivial, since β affects both the mass flow rate and the pressure ratio of the compressor.

2.3 Heat Exchanger Sizing

In aircraft applications, the size and mass of heat exchangers are critical as they affect packaging and integration, and aircraft efficiency. Therefore, it is a central metric for comparing the conditioning architectures. HX sizing is commonly assessed through the logarithmic mean temperature difference (LMTD) and the required heat transfer capability kA, that is the product of the overall heat transfer coefficient k and area A.

The LMTD generally defines the existing temperature difference between fluids exchanging energy. It is expressed as the temperature difference ΔT of one side *A* subtracted by the temperature difference of side *B*, divided by the logarithm of the ratio of temperature differences, given in Equation (1).

$$LMTD = \frac{\Delta T_A - \Delta T_B}{\ln\left(\frac{\Delta T_A}{\Delta T_B}\right)} \tag{1}$$

Between the cross-, counter-, and parallel-flow heat exchangers, the counter-flow heat exchanger is considered the most thermodynamically efficient, as it maximizes the LMTD compared with other HX designs.

The aforementioned required heat transfer capability of a HX is evaluated by setting the heat flow rate $\dot{Q}$ to the available driving temperature difference via $kA = \dot{Q}/LMTD$. Under the assumption of a constant overall heat transfer coefficient, a high kA therefore requires a large heat transfer area to dissipate a given amount of heat, indicating that a low kA will generally result in more compact heat exchanger sizing.

2.4 Definition of Compressor Placement and Parameter Studies

Parameter and sensitivity studies are used to investigate the H_2 conditioning architectures and the performance of their components. This will outline operational limits, performance and sizing trends and non-linearities, and supports the selection of preferable operating conditions and conditioning architectures.

2.4.1 Compressor Placement

Aforementioned, two distinct philosophies are distinguished for compressor placement. One minimizes the compressors operating temperature, keeping its power demand low, while the second maximizes the nitrogen's thermal energy available at the H2-N2-HX.

The power required by the compressor is given by the product of the mass flow rate and the specific enthalpy change across the machine, $P = \dot{m} \cdot \Delta h$. For a given pressure ratio, the enthalpy rise Δh is approximately proportional to the compressor inlet temperature, as warmer, less dense gas requires more specific work to reach the same pressure level. Higher inlet temperatures, as a consequence, result in a higher power demand at a given mass flow rate. The enthalpy rise is internally calculated via the isentropic/polytropic efficiency of the pressurization device at its current operating point.

By placing the nitrogen compressor downstream of the H2-N2-HX, its inlet temperature will be very low at a high density. An upstream placement of the nitrogen compressor will result in high inlet temperatures; thus, increasing the nitrogen's temperature at the H2-N2-HX's inlet resulting from the compressor's work input.

For compressor placement, this means that maximizing the LMTD at the H2-N2-HX will result in more compact HX sizing. Simultaneously, it is assumed that the compressor in front of the H2-N2-HX compensates for part of the thermal energy otherwise provided by the exhaust-gas recuperator to reach predefined hydrogen injection temperatures, reducing the required heat flow rate at the N2-EG-HX. As a result, exhaust-gas recuperator sizing can be reduced.

2.4.2 Design and Off-Design Parameter Study

Multiple parameter studies were conducted throughout this work to characterize the operating behavior and range of the conditioning architectures, summarized in Table 2. The focus of this paper is on the CR state and a H_2 injection temperature variation, printed in bold in Table 2 for distinction, to understand the working principle and performance differences of the architectures. Other studies performed will not be addressed further herein, as this would exceed the scope of this work.

Table 2 – Conducted parameter studies in design (CR) and off-design (MTO).

Operating point	Parameter	Range	Step
Design	**H_2 injection temperature**	**250 – 400 K**	**2.5 K**
Design	N_2 mass flow rate	2.3 – 3.7 kg/s	0.05 kg/s
Design	Parallel architecture mass flow ratios	0.50 – 0.70	0.005
Off-Design	Oil-cooler heat flow rate	10 – 380 kW	10 kW
Off-Design	Relative N_2 compressor speed	105 – 200 %	2.5 %

For the design study, high hydrogen injection temperatures are expected to improve the thermal efficiency and performance of the aircraft through improved mixing and a reduced energy input required to reach ignition. To assess the feasibility and impact on the components, the hydrogen injection

temperature is varied between $250\,\mathrm{K}$ and $400\,\mathrm{K}$ in steps of $2.5\,\mathrm{K}$. The boundary conditions and solver settings are kept identical across all simulations to ensure comparability between the architectures.

For each design case varying the H_2 temperature, an off-design simulation at MTO is subsequently performed, capturing the impact of the design hydrogen injection temperature on off-design feasibility and on the resulting design restrictions. The off-design analysis is restricted to the most promising architectures identified in the design study.

3. Results and Discussion

This section shows and discusses the results of the compressor position evaluation with a variation of hydrogen injection temperatures first, subsequently discussing the H_2 temperature parameter study. As the design point may outline preferable boundary conditions and operational procedures, the off-design analysis during MTO conditions will provide further insight into the feasibility of certain preferable design points and outline performance trade-offs alongside restrictions and limitations.

For the evaluations, key performance indicators in the form of (relative) required heat transfer capabilities of the heat exchangers and compressor power consumption are primarily discussed, with the hydrogen injection temperatures and operational range in off-design additionally analyzed.

3.1 Compressor Placement Analysis

Outlined in Section 2.4.1, a significant impact of the compressor position within the nitrogen cycle on the heat exchanger sizing and the whole architecture is expected. Both cases *A* (compressor placed downstream of the H2-N2-HX), and *B* (compressor placed upstream of the H2-N2-HX) are be compared to another for the parallel heat-exchanger arrangement (Figure 1c).

3.1.1 Compressor Power Demand

The required compressor power as a function of the hydrogen injection temperature for both positions is shown in Figure 2.

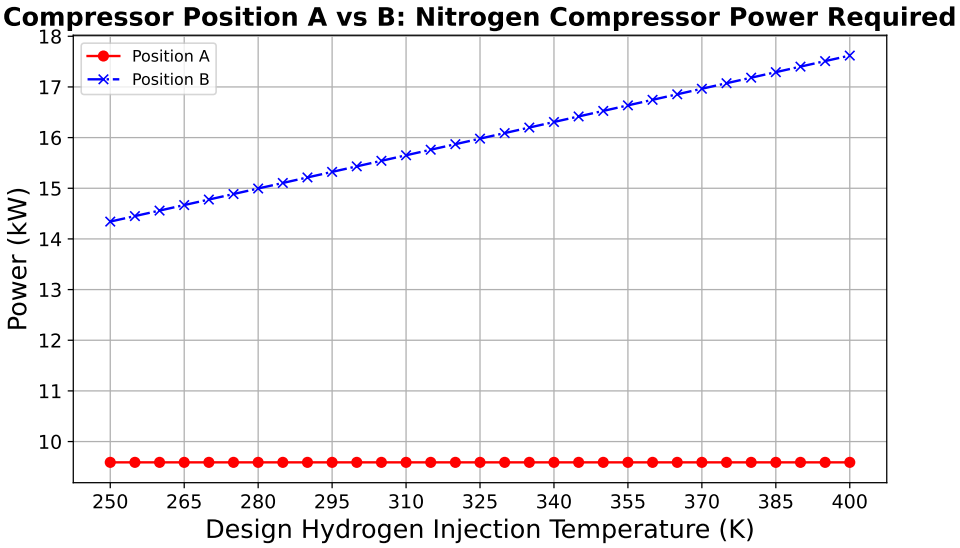


Figure 2 – A comparison of the compressor position's impact on the required compressor power as a function of the hydrogen injection temperature for the parallel HX arrangement.

The compressing power demand for configuration *A* remains below $10\,\mathrm{kW}$. Its inlet conditions are decoupled from the H_2 injection temperature, as the nitrogen temperature is limited to $273\,\mathrm{K}$ entering the N2-ECS- and N2-EG-HX with the icing constraint, requiring constant compressor inlet and outlet conditions. Configuration *B* rises steadily from approximately $14\,\mathrm{kW}$ to $18\,\mathrm{kW}$ as the H_2 injection temperature is increased from $250\,\mathrm{K}$ to $400\,\mathrm{K}$. Higher hydrogen temperatures require higher nitrogen inlet temperatures into the H2-N2-HX, raising the nitrogen's exit temperatures of the exhaust-gas

recuperator and consequently inlet temperatures into the compressor. Thus, for *B* the compressing power rises gradually with dependence on the hydrogen temperature, as more work is required to compress the fluid. Given the low overall power demand with respect to total engine shaft power, however, the negative impact on engine efficiency at elevated temperatures might be insignificant.

3.1.2 Impact on Nitrogen-Exhaust-Gas-Heat-Exchanger

Regarding the performance of the N2-EG-HX, the compressor placement has a complementary consequence. Figure 3 shows its LMTD and required kA for both positions. In *B*, the nitrogen is able to exit the N2-EG-HX cooler than in *A* yielding a consistently higher LMTD. By positioning the compressor upstream of the H2-N2-HX, the demanded energy input by the exhaust-gas is reduced, since the compressor compensates missing thermal energy.

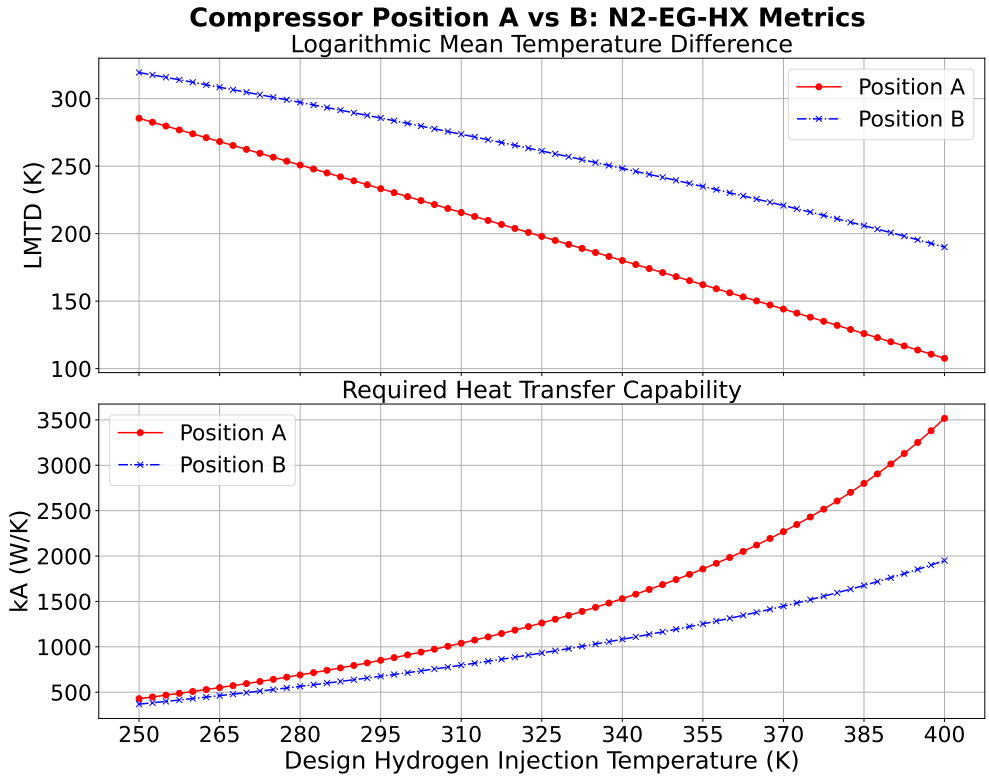


Figure 3 – A comparison of the compressor position's impact on exhasut-gas recuperators LMTD and *kA* as a function of the hydrogen injection temperature for the parallel arrangement.

Under the assumption that the overall heat transfer coefficient is similar for both simulations, the required kA, and therefore heat transfer area, drops by a substantial margin, with the largest deviation appearing at high H_2 injection temperatures, as the difference in LMTD increases. This behavior correlates with the additional work input by the compressor.

3.1.3 Sizing Impact on all Heat-Exchangers

The impact on the exhaust-gas recuperator is notable. An extended comparison considering all four heat exchangers is shown in Figure 4. Displayed is the relative deviation of each heat exchanger's kA of compressor position *A* to *B*. A value of $10\,\%$ e.g. indicates, that the considered HX in configuration *A* has to be designed $10\,\%$ larger than its counterpart with configuration *B* to equally fulfill its requirements. The oil cooler and N2-ECS-HX values are identical for both placements. Their boundary conditions ($T_{in} = 273\,\mathrm{K}$) are unaffected by the compressor position, as HX-icing must be prevented within those subsystems. The H2-N2-HX shows only a minor deviation. In contrast, the exhaust-gas recuperator, described previously, must be sized substantially larger in *A* – by approximately $50\,\%$ at a $360\,\mathrm{K}$ H_2 injection temperature – to compensate for the absent compressor-derived work input into the nitrogen and reduced LMTD. Across the studied hydrogen injection temperature range a total sizing increase between $17\,\%$ and $80\,\%$ is observed.

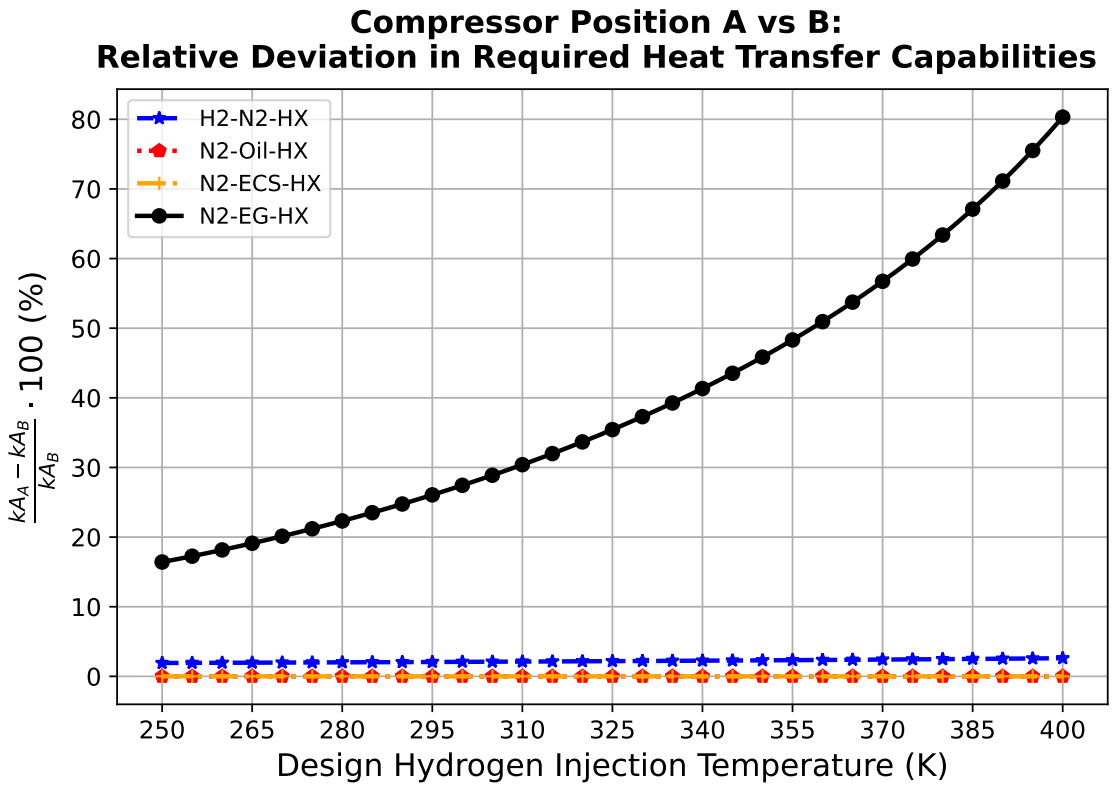


Figure 4 – Relative heat exchanger sizing differences as a function of the hydrogen injection temperature of the parallel configuration's compressor placement *A* compared with *B*.

In summary, configuration *B* trades a moderate increase in compressor power, for a substantially more compact N2-EG-HX. Whether the consequent heat exchanger weight reduction outweighs slightly increased pressurization power demands is not investigated within this study. The complete heat exchanger performance metrics at a hydrogen injection temperature of $300\,\mathrm{K}$ of the parallel architecture and both compressor positions are shown in Table 3 for further detail. ε denotes the HX effectiveness, defined as the ratio of the actual heat transfer rate to the maximum possible heat transfer rate, while the indexes *in*, *out*, and *PF* are short for inlet, outlet, and primary fluid (e.g. hydrogen), respectively.

Table 3 – HX performance metrics and compressor power for configurations *A P* and *B P* at a design H_2 injection temperature of $300\,\mathrm{K}$.

Component	**H2-HX**		**Oil-HX**		**ECS-HX**		**EG-HX**	
Comp. position	A	B	A	B	A	B	A	B
$\dot{Q}$ (kW)	449.7	449.7	157.0	157.0	76.00	76.00	207.1	201.3
kA (W/K)	2603	2550	2586	2586	285.4	285.4	910.8	714.7
$LMTD$ (K)	172.8	176.4	60.71	60.71	266.3	266.3	227.4	281.6
ε (-)	0.685	0.679	0.759	0.759	0.688	0.688	0.426	0.414
$\dot{m}_{N2}$ (kg/s)	2.700	2.700	1.306	1.306	0.179	0.179	1.215	1.215
$T_{in,N2}$ (K)	420.8	424.2	273.0	273.0	273.0	273.0	273.0	273.0
$T_{out,N2}$ (K)	269.5	273.0	381.3	381.3	661.4	661.4	427.7	423.2
$T_{in,PF}$ (K)	31.54	31.55	413.1	413.1	835.0	835.0	640.0	640.0
$T_{out,PF}$ (K)	300.0	300.0	376.4	376.4	660.3	660.3	516.3	631.4
P_{Comp} (kW)	A: 9.590				B: 15.43			

3.2 Comparison of Conditioning Architectures in Design

With compressor placement *B* showing significantly lower required heat transfer capabilities, the different HX arrangements and conditioning architectures are now compared to another for case *B*. The environments, being parallel *P*, semi-parallel *SP*, and serial *S*, differ in how the three heat sources are interconnected in the nitrogen loop, with direct consequences for the nitrogen temperature entering the H2-N2-HX and the required compressor power, as mentioned in Section 2..

3.2.1 Compressor Power Demand and its Nitrogen Inlet Temperatures

The compressor power demand is employed as the first performance metric again, next to the nitrogen temperature at its inlet to understand the main differences between the configurations. Figure 5 shows the nitrogen inlet temperature at the nitrogen compressor (left) and the required compressor power (right). *B P* operates at the highest nitrogen inlet temperature, approximately $50\,\mathrm{K}$ to $60\,\mathrm{K}$ above the other two arrangements. This results from the icing prevention and thus nitrogen inlet temperatures into the heat exhangers. In *B SP* and *B S*, the nitrogen first passes through the oil-cooler, which operates without a temperature limit; the icing constraint is only imposed downstream of the oil-cooler entering the N2-ECS- and N2-EG-HX, allowing the loop to operate at substantially lower temperature levels exiting the H2-N2-HX, consequently resulting in lower nitrogen inlet temperatures.

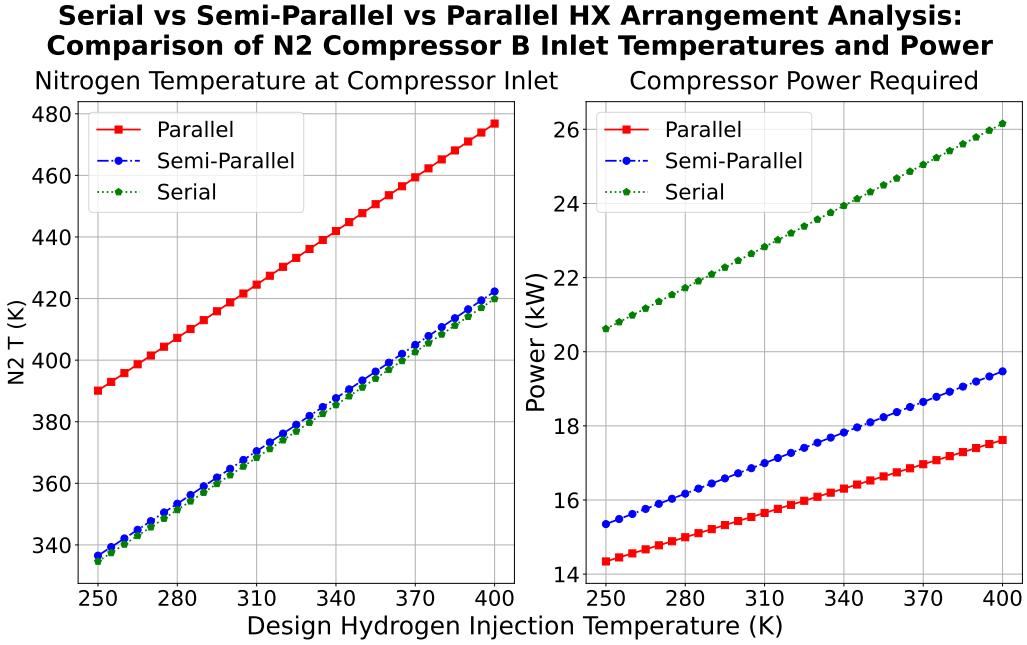


Figure 5 – Nitrogen temperatures at the compressor inlet and its corresponding power demand for each architecture as a function of the hydrogen injection temperature for compressor position *B*.

The compressor power follows an opposite order: *B P* requires the least, *B S* the most, with *B SP* in between. In contrast to the placement comparison, where the thermodynamic work governed the power demand, the major driver here is pressure loss, which increases for components placed in series. Hence greater pressure drops along the loop are accumulated, therefore demanding a higher pressure ratio from the compressor. The high pressure drop for the serial configuration qualitatively correlates well with the observed power input.

3.2.2 Impact on Heat-Exchanger Sizing

With the inlet temperature into the N_2 compressor reduced for the serial and semi-parallel arrangement, it is expected that there will be a negative impact on the H2-N2-HX caused by reduced LMTDs. The sizing demands for each heat exchanger related to the parallel study is illustrated in Figure 6.

The H2-N2-HX (top left) is the most architecture-sensitive component. In *B P*, the high nitrogen

inlet temperature yields a large LMTD and thus a low required heat transfer area, while *B SP* and *B S* both require a substantially larger H2-N2-HX due to their lower nitrogen inlet temperatures indicating a reduction in LMTD, as predicted. The remaining heat exchangers show the opposite trend. The oil-cooler and N2-ECS-HX can be sized between $40\,\%$ and $60\,\%$ smaller in *B SP* and *B S*, as the lower nitrogen temperatures and higher mass flow rates enable considerably higher LMTDs at these components. The exhaust-gas recuperator behaves differently across the arrangements. While *B S* yields no sizing gains because the nitrogen entering the EG-HX has already been heated by the upstream oil-cooler and N2-ECS-HX, reducing the available LMTD, *B SP* achieves minor reductions attributed to increased nitrogen mass flow rates passing the heat exchanger.

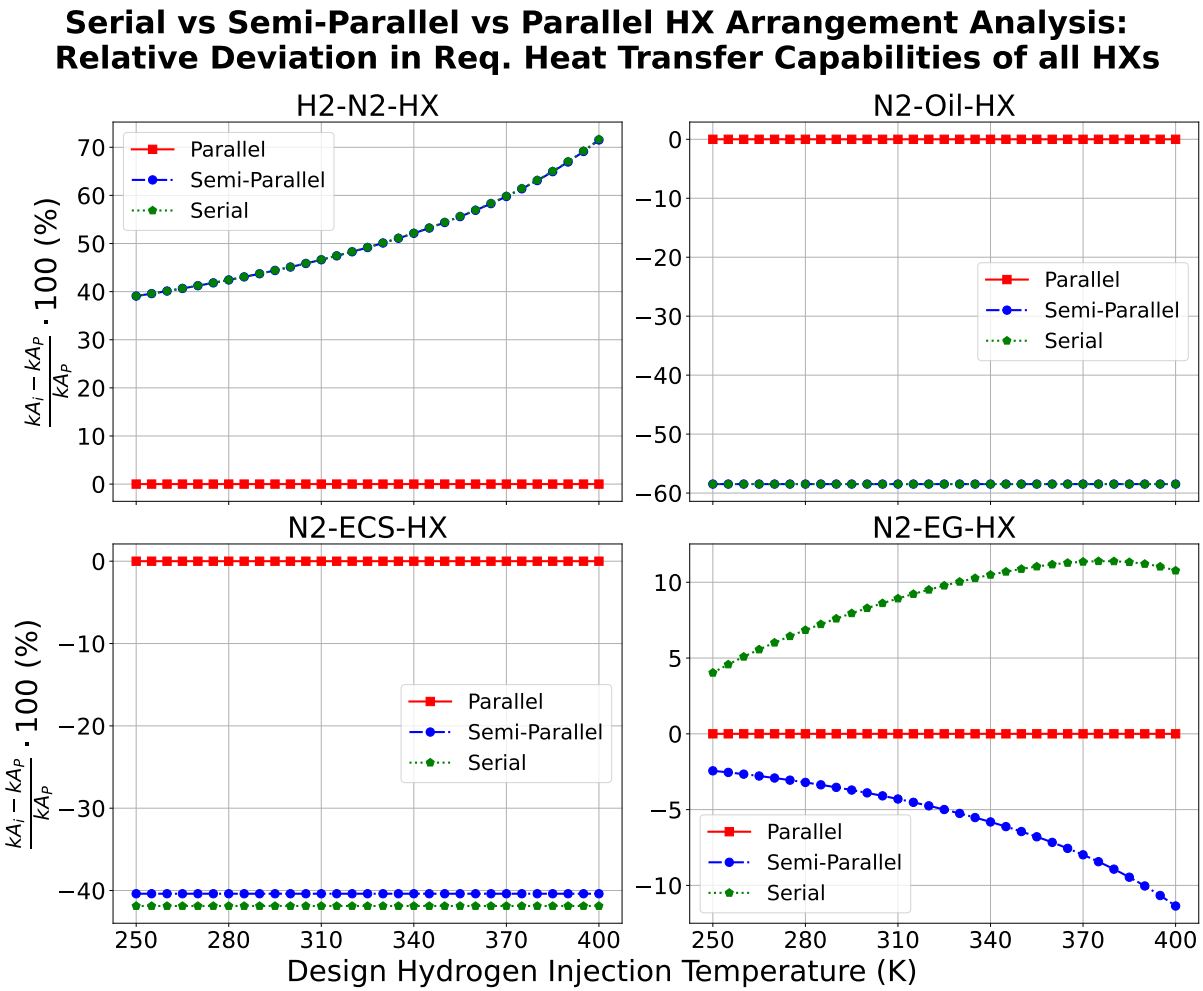


Figure 6 – Relative impact on each HX's *kA* as a function of the hydrogen injection temperature of the different conditioning architectures compared with the parallel configuration.

To consolidate these effects into a system-level metric, Figure 7 shows the kA-scaled relative deviation, referenced to *B P*. The kA-scaled comparison gives more weight to larger heat exchangers and therefore better reflects total mass and area savings. A slight exponential increase in relative size is observed for architecture *B P* and *B SP*, as the H2-N2-HX kA increase is larger than the reduction in others, seen in Figure 6. Below the crossover threshold at approximately $345\,\mathrm{K}$ hydrogen injection temperatures – assuming a constant overall heat transfer coefficient – *B SP* yields the least total required heat transfer area, driven by reductions in oil-cooler, N2-ECS-HX, and especially N2-EG-HX kA, closely followed by the serial architecture. Above $345\,\mathrm{K}$, the H2-N2-HX increasingly dominates the total area, and *B P* becomes preferable in terms of total HX compactness.

Both *B P* and *B SP* are carried forward to the off-design analysis in the following section, as both exhibit preferable properties at different temperature levels.

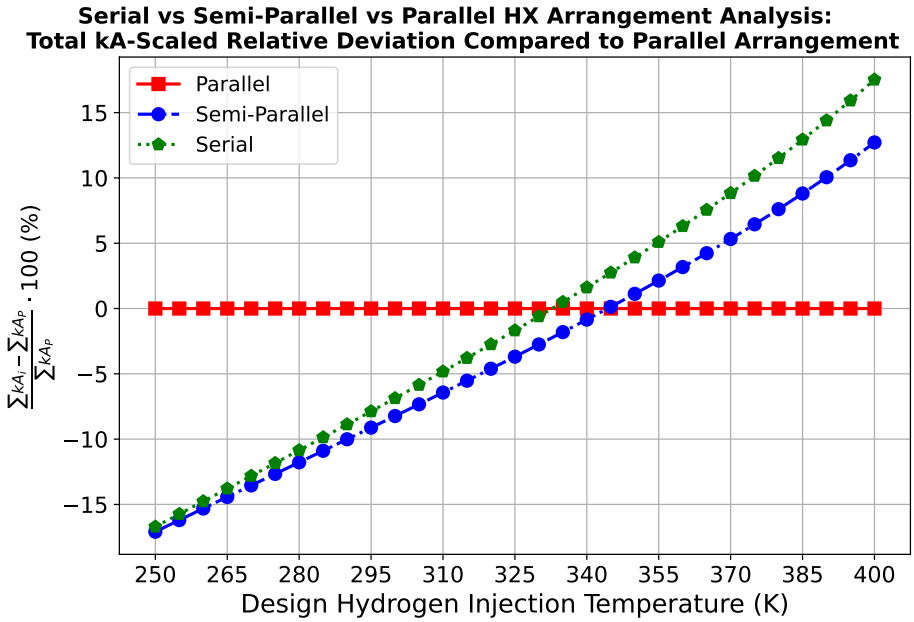


Figure 7 – Total kA-scaled relative deviation of the studied architectures as a function of the hydrogen injection temperature compared to the parallel configuration.

3.3 Comparison of Conditioning Architectures in Off-Design

For each design case of the two architectures retained from the design analysis – *B P*, and *B SP* – an off-design simulation at maximum take-off is performed. The oil-cooler and N2-EG-HX heat flow rates are fixed at $380\,\mathrm{kW}$ and $1\,\mathrm{MW}$ respectively, with the nitrogen temperature at the N2-EG-HX inlet again held at $273\,\mathrm{K}$ to prevent icing. The ECS is assumed to be inactive in the first stage of take-off.

3.3.1 MTO Hydrogen Injection Temperature

Similar to cruise flight, the hydrogen injection temperature during MTO should be sufficiently high for safe and stable operation. Figure 8 displays the MTO hydrogen injection temperature as a function of the design injection temperature.

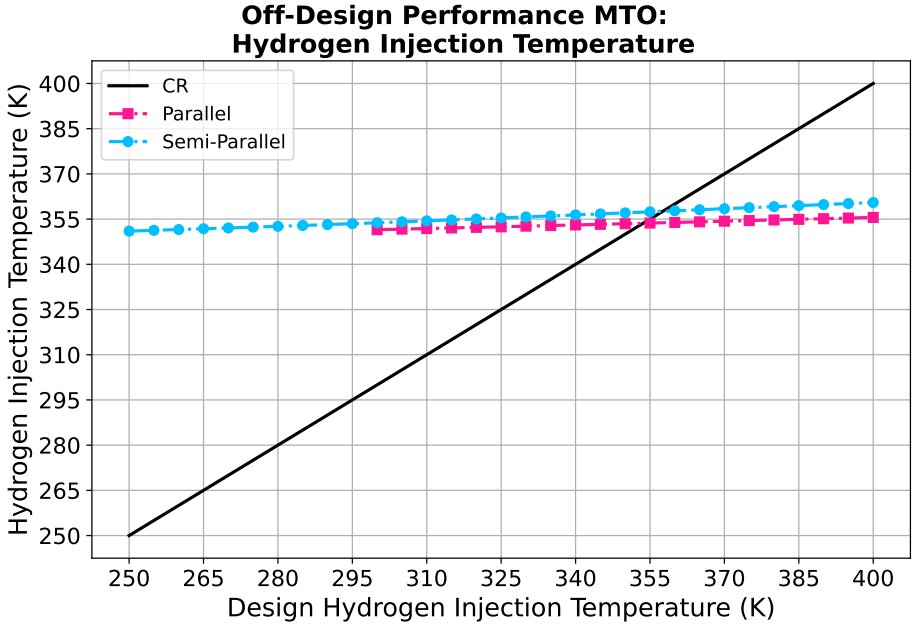


Figure 8 – MTO hydrogen inejction temperature as a function of the design hydrogen injection temperature of the parallel and semi-parallel conditioning architectures.

The MTO temperature stays within a comparatively narrow window, almost independent of the design injection temperature. *B SP* achieves the highest hydrogen temperatures across the entire range. *B P* becomes infeasible below a design temperature of approximately $300\,\mathrm{K}$ – the underlying cause is addressed in the subsequent heat exchanger analysis. Since the oil-cooler and N2-EG-HX heat flow rates are fixed, the variations in MTO hydrogen temperature are entirely attributed to the additional energy introduced by the compressor.

A constant heat flow rate delivery of $1\,\mathrm{MW}$ by the exhaust-gas might not represent real flight conditions, for first feasibility and overall system evaluations is acceptable.

3.3.2 Compressor Power Demand

Off-design compressor demand is more complex than the design case. The nitrogen mass flow rate is now varying according to engine speed, nitrogen temperatures, pressure losses and thermal demands. Therefore, the impact on power consumption is expected to be more significant than in design, proven in Figure 9. As the dissipated energy increases to $1\,\mathrm{MW}$ by the exhaust-gas, the nitrogen's mass flow must increase to absorb the given heat flow rate. With the compressor's operating point shifting due to changed inlet conditions, the compressor efficiency changes, likely operating at a less efficient level. Less efficient compressors, as a consequence, require a higher power input. Indicated in the figure, *B SP* requires the most compressing power, exceeding *B P* by almost $25\,\mathrm{kW}$ at high design H_2 temperatures. Thus, the impact of changed mass flow rates and operating points within the compressor map is substantial. Compared to design power demands, MTO exceeds them in a range of $200\,\%$ to $300\,\%$.

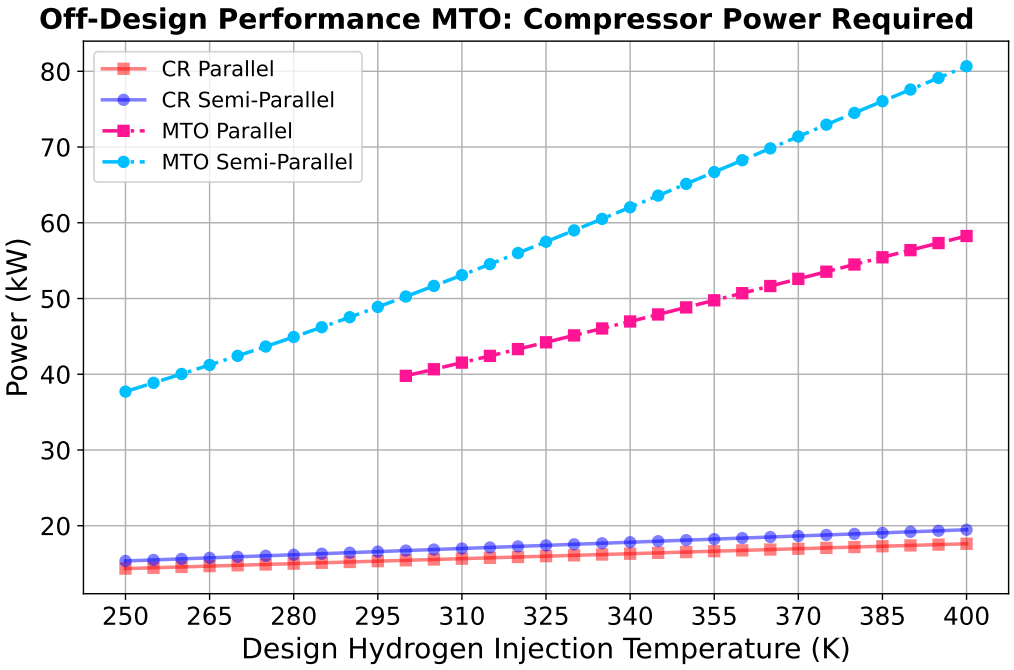


Figure 9 – MTO power demand as a function of the design hydrogen injection temperature of the parallel and semi-parallel conditioning architectures.

3.3.3 Heat Exchanger Impact

Since the heat exchangers are sized in design, the heat transfer area is fixed in off-design and the overall heat transfer coefficient must adjust to meet the heat transfer requirements. The required k-scaling factor – defined as the ratio of MTO to design overall heat transfer coefficient – is shown in Figure 10 for the H2-N2-HX (top) and N2-EG-HX (bottom). The oil-cooler is omitted, as it does not show a limiting behavior.

Across all cases the k-scaling factors decrease as the design hydrogen temperature rises but stays consistently above unity, meaning the heat exchangers must over-perform at MTO. For the exhaust-gas recuperator, the parallel configuration *B P* exhibits a strongly negative slope at low design H_2 injection temperatures, indicating that the required HX effectiveness approaches unity and would exceed it below a temperature of $300\,\mathrm{K}$. The decreasing trend observed is resulting from larger heat exchangers defined in the design point for high H_2 temperatures, since more energy needs to be dissipated into the nitrogen. As an example, low hydrogen injection temperatures indicate a small N2-EG-HX, making it impossible for the heat exchanger to transfer the given amount of heat. If these low H2 temperatures are desired, the N2-EG-HX needs to be oversized, thus underperforming in its design state, which is not desired.

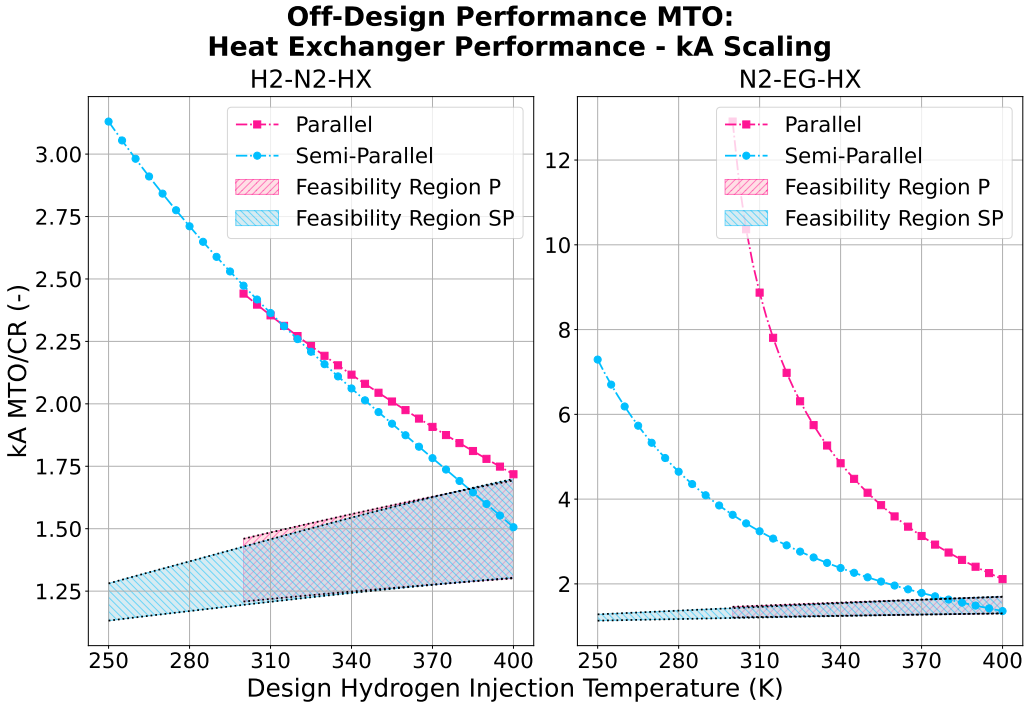


Figure 10 – *kA* requirements in MTO compared to the design point for the H2-N2-, and N2-EG-HX as a function of the design hydrogen injection temperature of the parallel and semi-parallel conditioning architectures.

In contrast, *B SP* exhibits a more favorable behavior, with low k-scaling factors and, therefore, exhaust-gas recuperator effectiveness well below unity across the entire studied range. Since the overall heat transfer coefficient is unable to be scaled infinitely but by a certain factor, high design hydrogen injection temperatures are preferable, as they bring the required heat transfer coefficients closer to physically realizable values. Generally, the overall heat transfer coefficient, in dependence on its design value k_{design}, scales by the mass flow rate $\dot{m}$, given in Equation (2) (cf. [26])

$$k = k_{design} \cdot \left(\frac{\dot{m}}{\dot{m}_{design}} \right)^{n}, \tag{2}$$

with the exponent *n* depending on the fluid properties and governed flow regime, typically between 0.4 and 0.8 (cf. [27]).

Evaluated data from other configurations suggest that, in off-design conditions, the parallel architecture with the compressor in its position *A* performs better than its counterpart. This behavior can be attributed to increased N2-EG-HX sizing demands in design. In fact, considering each conditioning architecture with each compressor position, architecture *A P* showed the highest total kA of all concepts, only being surpassed by the serial case with compressor *A* at design hydrogen injection temperatures beyond $340\,\mathrm{K}$.

Throughout additional simulations, environment *B SP* proved to be the most versatile in terms of operability with compressor map restrictions and HX limitations, similar to the results shown herein. The only downside observed thus far is its increased power consumption compared to other architectures.

4. Conclusion and Outlook

This work assessed liquid-hydrogen conditioning architectures for combusting aero-engine applications employing exhaust gas waste heat recovery, summarizing selected results from a broader thesis investigation (cf. [28]). A secondary cycle with nitrogen introduced as the heat transfer fluid emits heat into the hydrogen after being warmed by the integrated engine oil-cooler, bleed-air cooler for application in the environmental control system, and EG heat exchanger. Three hydrogen conditioning architectures with differing arrangements of the heat exchangers – serial *S*, semi-parallel *SP*, and parallel *P* – combined with two nitrogen compressor positions for fluid delivery (downstream and upstream of the H2-N2-HX) were compared. A design study at cruise flight conditions varied the hydrogen injection temperature between $250\,\mathrm{K}$ and $400\,\mathrm{K}$, and an off-design study at maximum take-off captured the system response dependent on design conditions and thus component sizing, assessing operational feasibility and consequent design limitations. The hydrogen and exhaust-gas heat exchangers were identified as the components most sensitive to the architecture choice.

The design study showed that placing the nitrogen compressor upstream of the H2-N2-HX (case *B*) consistently yields more compact heat exchangers compared with a downstream placement, at the cost of a moderate compressor power penalty. The two most promising arrangements are *B P* and *B SP*. Below approximately $345\,\mathrm{K}$ design hydrogen temperature, *B SP* delivers the smallest total heat transfer area, driven by substantial size reductions of the oil-cooler and N2-ECS-HX. Above this threshold, *B P* becomes preferable as the H2-N2-HX increasingly dominates the total required heat transfer area.

The off-design analysis revealed that high design hydrogen injection temperatures are essential for operability at MTO, since the required scaling factor of the overall heat transfer coefficient drops to physically realizable values only at elevated design hydrogen injection temperatures. Neglecting the overall heat transfer coefficient requirement, *B P* generally becomes infeasible below $300\,\mathrm{K}$ design hydrogen temperatures, where the N2-EG-HX effectiveness would have to exceed unity. Additional findings from an oil-cooler heat flow rate parameter study confirmed *B SP* as the most stable architecture across the transition from idle to MTO thrust, where the oil-cooler heat flow rate continuously increases, with viable overall heat transfer coefficient scaling factors at all operating points.

An off-design study of the relative compressor speed – which was held constant at $130\,\%$ for discussed simulations – revealed a trade-off emerging between increased hydrogen injection temperatures in off-design and compressing power. An increase in compressor power of $200\,\mathrm{kW}$ corresponds to a temperature rise of $60\,\mathrm{K}$. Whether the engine-side performance gain outweighs the power-consumption penalty remains to be quantified. Further, with increasing compressor speeds, the nitrogen temperature entering the H2-N2-HX decreases, reducing the overall heat transfer coefficient scaler for the N2-EG-HX, with an increasing overall heat transfer coefficient required at the H2-N2-HX resulting from lowered LMTDs.

Several modeling assumptions limit the generality of these results. The overall heat transfer coefficient was assumed as constant in design across architectures. Resolving the heat transfer area and the coefficient separately, and implementing a physics-based scaling in GTlab, would substantially improve fidelity. The exhaust-gas recuperator heat flow rate was held constant in off-design to isolate architecture effects; in practice it would adjust to satisfy MTO scaling constraints, which may alter the architecture ranking. The hydrogen conditioning system was uncoupled from the engine, thus only boundary conditions at specified interfaces were defined. Full engine coupling will provide more insight as flight phases and effects on engine performance are better resembled, which was

conducted by Görtz et al. [16] subsequently to the present study. Pressure drops caused by the exhaust-gas recuperator might even reduce total thrust, thus impacting the performance of conditioning architectures, as the work of Lu et al. [13] showed, substantiating the importance of full engine coupling. A separate weight and sizing estimation of each component will give additional insight into viability of the results, with first heat exchanger modeling methods provided by Görtz et al. [29] for hydrogen powered aero engines.

5. Contact Author Email Address

philip.kirschnek@fh-joanneum.at

6. Copyright Statement

The authors confirm that they, and/or their company or organization, hold copyright on all of the original material included in this paper. The authors also confirm that they have obtained permission, from the copyright holder of any third party material included in this paper, to publish it as part of their paper. The authors confirm that they give permission, or have obtained permission from the copyright holder of this paper, for the publication and distribution of this paper as part of the ICAS proceedings or as individual off-prints from the proceedings.

References

[1] Overton J. U.S. and International Commitments to Tackle Commercial Aviation Emissions, 2025.

[2] European Aviation Safety Agency. EUROPEAN AVIATION ENVIRONMENTAL REPORT, 2025.

[3] Brewer G D, Morris R E, Davis G W, Versaw E F, Cunnington Jr G R, Riple J C, Baerst C F, and Garmong G. *Study of fuel systems for LH2-fueled subsonic transport aircraft, volume 1*. 1978.

[4] Faaß R. Cryoplane: Flugzeuge mit Wasserstoffantrieb, 2001. presentation.

[5] Airbus. ZEROe: our hydrogen-powered aircraft, 2025.

[6] Brewer G D. *Hydrogen aircraft technology*. Routledge, 2017.

[7] Sosounov V and Orlov V. Experimental turbofan using liquid hydrogen and liquid natural gas as fuel. *26th Joint Propulsion Conference*, 1990.

[8] Boeing. Boeing 'Phantom Eye' Hydrogen Powered Vehicle Takes Shape, 2010.

[9] Tiwari S, Pekris M J, and Doherty J J. A review of liquid hydrogen aircraft and propulsion technologies. *International Journal of Hydrogen Energy*, 57:1174–1196, 2024.

[10] Esgar J B. State of technology on hydrogen fueled gas turbine engines, 1974.

[11] Capitao Patrao A, Xisto C, Jonsson I, and Lundbladh A. ENABLEH2 D2.4 - Final report on heat management system, 2023.

[12] Tang X and Shen S. Airworthiness Compliance Design of Liquid Hydrogen Heat Exchangers for Aero Hydrogen Turbine Engines. In *Proceedings of the 7th China Aeronautical Science and Technology Conference*, pages 395–403, Singapore, 2025. Springer Nature Singapore.

[13] Lu B, Shi L, Wang M, Xiong S, Zhang J, Peng J, and Han K. Exhaust Heat Recovery for Cryogenic Hydrogen-Powered Aircraft: From Conceptual Design to Experimental Validation. *Engineering*, 2025.

[14] Abedi H, Xisto C, Jonsson I, Grönstedt T, and Rolt A. Preliminary Analysis of Compression System Integrated Heat Management Concepts Using LH2-Based Parametric Gas Turbine Model. *Aerospace*, 9(4), 2022.

[15] Deutsches Zentrum für Luft- und Raumfahrt e.V. Gtlab - gas turbine laboratories.

[16] Görtz A, Häßy J, Schmelcher M, El-Soueidan M, and Herbst F. Integration of a Liquid Hydrogen Conditioning System into the Performance Calculation of a Turbofan Engine using a Secondary Fluid. In *Proceedings of ASME Turbo Expo*, Milan, Italy, 2026.

[17] Corchero G and Montañés J L. An approach to the use of hydrogen for commercial aircraft engines. *Proceedings of the Institution of Mechanical Engineers, Part G*, 219(1):35–44, 2005.

[18] Gkantonas S, Talibi M, Balachandran R, and Mastorakos E. *Hydrogen Combustion in Gas Turbines*, pages 407–428. Springer International Publishing, Cham, 2023.

[19] Capitao Patrao A, Jonsson I, Xisto C, Lundbladh A, and Grönstedt T. Compact heat exchangers for hydrogen-fueled aero engine intercooling and recuperation. *Applied Thermal Engineering*, 243:122538, 2024.

[20] Canière H, Willockx A, Dick E, and De Paepe M. Raising cycle efficiency by intercooling in air-cooled gas turbines. *Applied Thermal Engineering*, 26(16):1780–1787, 2006.

[21] Sciatti F, Di Domenico V, Tamburrano P, Distaso E, and Amirante R. An Innovative Cryogenic Heat Exchanger Design for Sustainable Aviation. *Energies*, 18(5), 2025.

[22] Görtz A and Silberhorn D. Thermodynamic Potential of Turbofan Engines with Direct Combustion of Hydrogen. In *33rd Congress of the International Council of the Aeronautical Sciences*, Stockholm, Sweden, 2022.

[23] Bell I H, Wronski J, Quoilin S, and Lemort V. Pure and pseudo-pure fluid thermophysical property evaluation and the open-source thermophysical property library coolprop. *Industrial & Engineering Chemistry Research*, 53(6):2498–2508, 2014.

[24] Exxon Mobil aviation. Mobil Jet™Oil II. `https://www.exxonmobil.com/en-us/aviation/pds/gl-xx-mobil-jet-oil-ii`, 2025. Cited: 02 June 2026.

[25] Patnaik P. *A Comprehensive Guide to the Hazardous Properties of Chemical Substances*. John Wiley & Sons, 2007.

[26] Schmelcher M, Görtz A, Häßy J, El-Soueidan M, and Nöske F T. Integration of Heat Exchanger Models into the Performance Analysis of Innovative Aero Engine Architectures. *International Society of Air Breathing Engines*, 2024.

[27] Jørgensen P H, Ommen T, Markussen W B, and Elmegaard B. Performance Optimization of a Large-Scale Ammonia Heat Pump in Off-Design Conditions. In *8th Conference on Ammonia and CO2 Refrigeration Technologies*, pages 107–114. International Institute of Refrigeration, 2019.

[28] Kirschnek P. Modeling and Evaluation of LH2 Conditioning Concepts in the Exhaust Gas Stream of Aircraft Engines. Master's thesis, FH JOANNEUM, September 2025.

[29] Görtz A, Häßy J, Baier Schmelcher M, El-Soueidan M, and Herbst F. Heat Exchanger Modelling Methods for Hydrogen Powered Aero Engines during Thermodynamic Cycle Design. In *35th Congress of the International Council of the Aeronautical Sciences*, Sydney, Australia, 2026.